

# DESIGN PROCEDURE AND HONEYCOMB SCREEN IMPLEMENTATION TO THE AIR TRANSPORT DEPARTMENT'S SUBSONIC WIND TUNNEL

**Michal Hruz**  
Air Transport Department  
University of Žilina  
Univerzitná 8215/1  
010 26, Žilina  
michal.hruz@stud.uniza.sk

**Pavol Pecho**  
Air Transport Department  
University of Žilina  
Univerzitná 8215/1  
010 26, Žilina  
pavol.pecho@fpedas.uniza.sk

**Martin Bugaj**  
Air Transport Department  
University of Žilina  
Univerzitná 8215/1  
010 26, Žilina  
martin.bugaj@fpedas.uniza.sk

## Abstract

Wind tunnels are the most widely used tools when comes to validation of Reynold number. Most of wind tunnels use various air straighteners or flow conditioners to achieve as most unified air flow as it's possible. This article deals with design and creation procedure of air flow straightener – honeycomb screen. Based on mathematical relations and empirical experience defines dimensions and characteristics for subsonic wind tunnel of the Air Transport Department of University of Žilina. Wind tunnel equipped with a suitable screen provides more relevant and accurate data, which are crucial for final validation of results of test objects.

## Keywords

honeycomb, air straightener, flow conditioner, flow straightener, screen, wind tunnel

## 1. Introduction

The wind tunnel is a tool to study fluid flows around a body and the forces generated by the fluid-structure interaction (Panda & Samanta, 2016). The main concerns of aircraft aerodynamics are reducing drag, reducing noise, and improving lift forces on aerodynamic objects (Łusiak, 2020). Wind tunnels are used as a key tool in various engineering applications such as building aerodynamics, study of boundary layers, simulation of atmospheric layers, small-scale testing of aircraft/vehicle models and subsequent validation of numerical predictions. They offer a rapid, economical, and accurate means for aerodynamic research (Kulkarni et. al., 2011).

The Reynolds ( $Re$ ) number is a quantity which engineers use to estimate if a fluid flow is laminar or turbulent. This is important, because increased mixing and shearing occur in turbulent flow. The Reynolds number is calculated using mean velocity, pipe diameter, density, and viscosity, and is valid for any fluid. The Reynolds number is also dependent upon the geometry of the pipe, as well as the roughness of the walls. Yet, no successful analytical methods for determining the Reynolds number have been developed due largely to the difficulty associated with predicting turbulent flow, and so Reynolds numbers for flow through pipes or around immersed objects must be determined experimentally (Yang, 2012).

In view of this necessity, a subsonic wind tunnel has been installed at Žilina Airport in Dolný Hričov in the year 2020. The layout of this tunnel with the dimensions of various components is shown in Fig. 1.

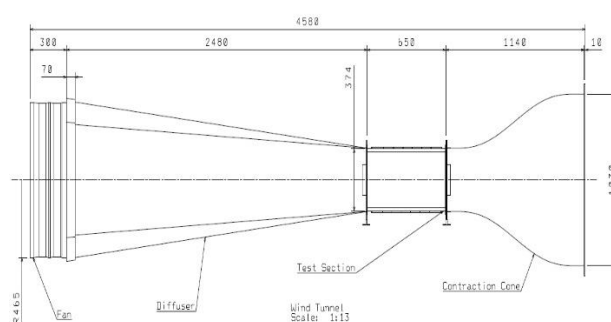


Figure 1: Layout of the subsonic wind tunnel at Žilina Airport, Dolný Hričov. Source: Authors.

It is an open-circuit type wind tunnel with a square test section of  $0.35 \times 0.35 \text{ m}^2$  and  $0.650 \text{ m}$  length. Air flow is established in the test section by using an axial fan powered by  $400 \text{ W}$  electric motor. This subsonic wind tunnel consists of four segments or sections. The inlet section and diffuser are made of laminated wood. The process of lamination was done with the usage of five levels of plywood, which were glued together in special forms in order to establish curved profiles.

In terms of simplicity of construction and economy, the bearing structure of the test section, which is shown in Fig. 2., is composed of aluminium strips, which were welded to the desired profile. To ensure thorough visibility of the air flow inside, the walls of the test section are fitted with LED light elements and acrylic glass, which reinforces the structure and dampens possible vibration.

Generally, in order to achieve better performance in terms of laminar flow in the test section various methods can be

applied. The air straighteners or screens are often used mainly to minimize the turbulence level in the test section.

According to (Škultéty, 2018), the lower the Reynolds number the more laminar airflow can be expected.



Figure 2: Transparent test section. Source: Authors.

The screens cascade large-scale turbulent fluctuations into smaller scales. These decay in the settling duct must be sufficiently long to allow sufficient decay, while minimizing boundary-layer growth (Cattafesta, 2010).

According to (Kulkarni et. al., 2011) honeycomb is a passage of ducts, laid along the axis of the main air stream to suppress the cross velocity components, which are initiated during the swirling motion in the air flow during entry, The cross-sectional shapes of honeycombs may be square, circular and regular hexagonal cells, as shown in Fig. 3.

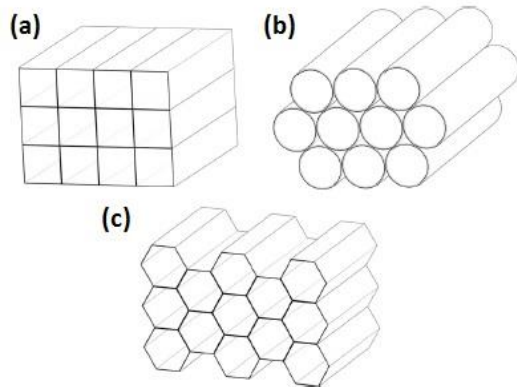


Figure 3: Schematic of several honeycomb cross-sections including square (a), circular (b) and regular hexagonal cell (c). Source: Kulkarni (2011).

## 2. Honeycomb design criteria

To improve the relevance of output data, it is necessary to design and create an optimal screen suited for the conditions of this wind tunnel.

According to (Metha & Bradshaw, 1979), as far as the design method is concerned, the honeycomb length, the cell hydraulic and the porosity are design key factors.

The honeycomb porosity is the ratio between the actual flow cross-section area and the total cross-section area, and it is expressed by Eq. (1).

$$\beta_h = \frac{\Omega_{Flow}}{\Omega_{tot}} \quad (1)$$

Two main conditions must be verified in the honeycomb design (Metha & Bradshaw, 1979). The honeycomb length and cell hydraulic diameter ratio must be in the range between 6 and 8 and the honeycomb porosity should be greater than 0.8 (see Eq. (2) and Eq. (3))

$$6 \leq \frac{L_{honey}}{d_{honey}} \leq 8 \quad (2)$$

$$\beta_h \geq 0.8 \quad (3)$$

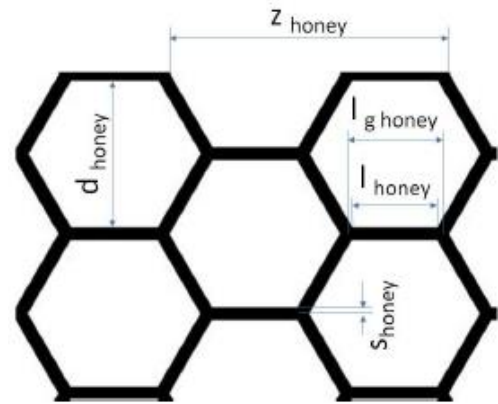


Figure 4: Honeycomb structure dimensions. Source: Mauro (2017).

As shown in Fig. 4, the honeycomb screen is defined by its geometric dimensions such as: inside honeycomb cell length  $l_{honey}$ ; outside honeycomb cell length  $l_g \text{ honey}$ ; honeycomb cell diameter  $d_{honey}$ ; honeycomb cell thickness  $S_{honey}$ ; honeycomb solid sheet divisions  $z$  (Mauro, 2017).

The internal and external honeycomb cell lengths may be determined thorough Eq. (4) and Eq. (5), respectively.

$$l_{honey} = \frac{d_{honey}}{2 \sin 60^\circ} \quad (4)$$

$$l_{g \text{ honey}} = l_{\text{honey}} + 2 \frac{S_{\text{honey}}}{\tan 60^\circ} \quad (5)$$

The solid sheet divisions can be evaluated using the same method (see Eq. (6)).

$$z_{\text{honey}} = 2 l_{\text{honey}} + 2 l_{g \text{ honey}} \quad (6)$$

In order to calculate the solid area of the honeycomb, considering a single division, the solid area is the sum of two rectangular areas and two trapezoidal areas (see Fig. 3.). These areas can be calculated using Eq. (7) and Eq. (8).

$$S_{\text{trapeze}} = l_{\text{honey}} S_{\text{honey}} \quad (7)$$

$$S_{\text{trapeze}} = \frac{(l_{\text{honey}} + l_{g \text{ honey}}) S_{\text{honey}}}{2} l_{\text{honey}} + l_{g \text{ honey}} \quad (8)$$

To determine the honeycomb porosity, it is necessary to determine the number of divisions height-wise and width-wise. The number of divisions height-wise is defined as the ratio between the settling chamber cross-section height and the honeycomb divisions, as showed in Eq. (9).

$$n_z = \frac{h_{SC}}{z_{\text{honey}}} \quad (9)$$

The number of divisions width-wise is the ratio between the settling chamber cross-section width and the sum of honeycomb cell thickness and the half honeycomb cell diameter (see Eq. (10)).

$$n_{\text{sheet}} = \frac{L_{SC}}{h_{SC} + \frac{d_{\text{honey}}}{2}} \quad (10)$$

It is evident that for square cross-sections Eq. (11) comes out.

$$h_{SC} = L_{SC} \quad (11)$$

Therefore, the cross-section area of the honeycomb solid sheet is calculated using Eq. (12).

$$\Omega_{\text{sheet}} = 2 (S_{\text{rectangle}} + S_{\text{trapeze}}) n_z n_{\text{sheet}} \quad (12)$$

In a dual way, it is possible to define the honeycomb solidity as the ratio between the cross-section area of the solid sheet and the settling chamber cross-section area. According to the solidity definition, Eq. (13) comes out.

$$\sigma_h = \frac{\Omega_{\text{sheet}}}{\Omega_{\text{tot}}} \quad (13)$$

Comparing Eq. (13) and Eq. (19), it is easy to achieve the conclusion that the honeycomb and porosity are complementary factors. Thus, Eq. (14) comes out.

$$\sigma_h + \beta_h = 1 \quad (14)$$

Therefore, knowing the honeycomb solidity, the porosity can be calculated using Eq. (14). Thus, the criterion expressed in Eq. (3) is verified.

The design criterion in Eq. (2) should be verified. Thus, the cell hydraulic diameter should be calculated. Firstly, the cell area is calculated using Eq. (15).

$$\begin{aligned} \Omega_{\text{cell}} &= 6 \left( \frac{d_{\text{honey}} l_{\text{honey}}}{2} \right) = 6 \frac{d_{\text{honey}} d_{\text{honey}}}{2 \cdot 2\sqrt{3}} \\ &= \frac{3 d_{\text{honey}}^2}{2 \sqrt{3}} \end{aligned} \quad (15)$$

Areas equality is used (see Eq. (16)) to determine the cell hydraulic diameter.

$$\pi \frac{D_h^2 d_{\text{honey}}}{4} = \Omega_{\text{cell}} = \frac{3 d_{\text{honey}}^2}{2 \sqrt{3}} \quad (16)$$

Thus, Eq. (17) comes out and the cell hydraulic diameter can be obtained.

$$D_{h \text{ honey}} = d_{\text{honey}} \sqrt{\frac{6}{\pi\sqrt{3}}} \quad (17)$$

It should be noted, that both criteria expressed by Eq. (2) and Eq. (3) must be verified at the end of the honeycomb design procedure.

### 3. Installation criteria

Final screen was placed into straight section which is part of the inlet section. The straight section provides almost 0.14 m long space right in front of the test section. The diameter of the straight section is the same as the test section, 0.35 x 0.35 m.

Based on the mentioned in the previous chapter, the final dimensions of honeycomb were set as is shown in Tab. 1. and Fig. 5.

Table 1: Final dimensions of honeycomb screen. Source: Authors.

| Criteria             | Value               |
|----------------------|---------------------|
| Criterion 1. Eq. (2) | $6 \leq 7.5 \leq 8$ |
| Criterion 1. Eq. (3) | $0.94 \geq 0.8$     |
| Screen length        | 83 mm               |
| $l_{\text{honey}}$   | 7 mm                |
| $l_{\text{g honey}}$ | 7.8 mm              |
| $d_{\text{honey}}$   | 13.6 mm             |
| $S_{\text{honey}}$   | 0.8 mm              |

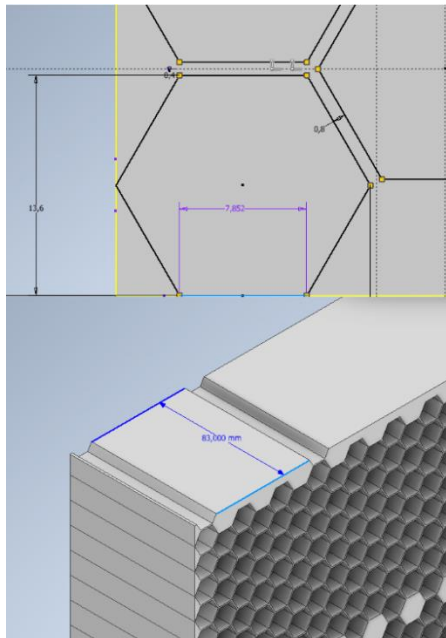


Figure 5: Printing design of honeycomb in PC software Inventor 2019. Source: Authors.

Due to financial costs and simplicity the honeycomb screen itself was 3D printed using FDM method, which is the most frequent method for printing 3D objects such as functional prototypes and concept models (Pecho, 2019). It involves melting the working material and applying it with thin threads one on top of the other. When it freezes, the material binds together to form a hard and durable coating (Iljaszewicz, 2020). Because of the large size of the honeycomb screen, the whole printing process was divided into four individual parts (see fig. 6.).

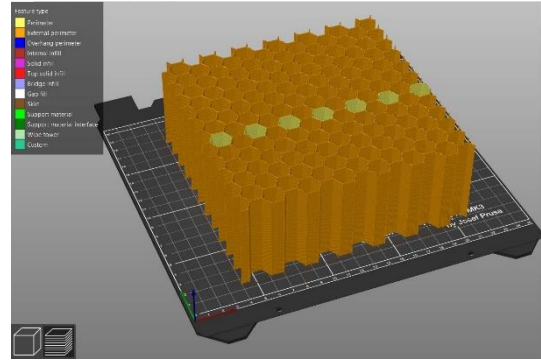


Figure 6: Printing design of one part of four. Source: Authors.

All four parts were glued together and create the final form of honeycomb screen. In order to remove possible roughness after the print, all surfaces were subjected to mechanical treatment.

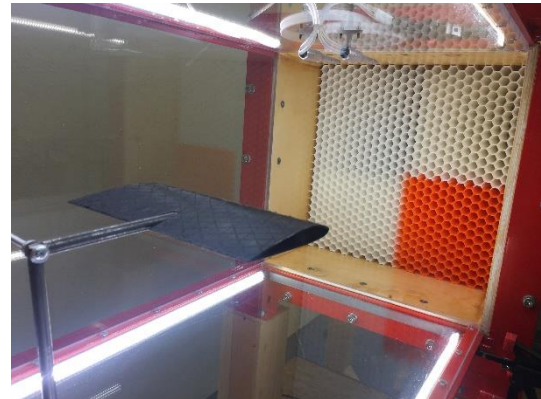


Figure 7: Final form of honeycomb screen installed in straight section. Source: Authors.

Sides of the honeycomb were designed to have tapered profile so it can fit right into a straight section of the inlet section (see Fig. 7.). This option reduced the possibility of vibration or incorrect placement of the screen. In addition, the smoke nozzles are located right behind the air straightener, thus the air mixed with a smoke can easily access to the its cells.

#### 4. Results

Verification of velocity and laminar flow was performed after the installation of honeycomb screen. Verifications were carried out by usage of anemometer, which is a device used for measuring wind speed (air velocity) and in form of visual check.

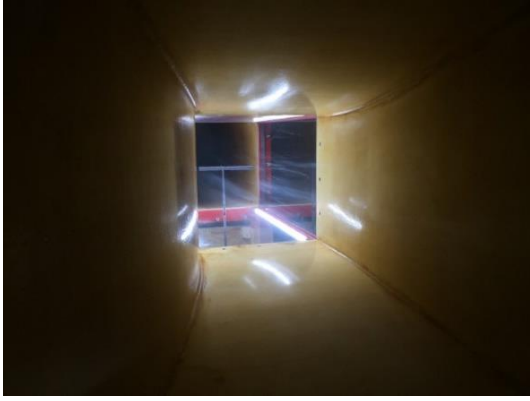


Figure 8: Air flow before the installation of air straightener. Source: Authors.

The Fig. 8. shows how the air flow looked before the installation of air straightener. The air flow is separated. Individual streamlines are separated from each other in the test section all around the tested wing profile, which presents unwanted conditions for relevant outputs of experimental measurement and visual analyses.



Figure 9: Air flow visualisation after the installation of honeycomb screen. Source: Authors.

Installation of honeycomb screen made a significant improvement in the terms of laminar flow inside the test section as we can see in Fig. 9., individual streamlines create one uniform stream or air flow which over floats tested wing profile.

However, the drawback of this improvement is the air velocity loss. The anemometer showed huge reduction of air velocity inside the test section. Before the installation, the wind tunnel could reach speed of almost 11.1 m/s (40 km/h). After the installation, the speed was reduced almost twice. Anemometer showed only 6.9 m/s (25 km/h).

## 5. Conclusion

In conclusion, it is possible to claim that the main goal was successfully fulfilled. On the other hand, the size of the honeycomb screen itself is responsible for huge air velocity drop inside the test section, mainly because it creates unwanted drag.

In order to achieve higher air velocity inside the test section, it is suggested to replace an axial fan which was powered by 400 W electric motor for a stronger one. The wind tunnel meets the specified criteria for running the experiments. The aim of

the paper was to describe the design and structure of the honeycomb screen construction for specific requirements and conditions, specifically for the subsonic wind tunnel of Air Transport Department of The University of Žilina. During the design phase, the authors followed mathematical methods for calculating the dimensions of open-type subsonic wind tunnels.

## Future work

A new stronger electric motor is currently being installed along with the frequency converter. The old 400 W electric engine will be replaced for a new 4 kW electric engine. The 10 times stronger fan can provide enough power a thus air velocity for experimental analysis in subsonic wind tunnel.

## Acknowledgment

This work was supported under the project of Operational Programme Integrated Infrastructure: *Research and development of contactless methods for obtaining geospatial data for forest monitoring to improve forest management and enhance forest protection, ITMS code 313011V465*. The project is co-funding by European Regional Development Fund.

## References

- Cattafesta, L. & Bahr, C., et. al., Fundamental of Wind-Tunnel design. Encyclopedia of Aerospace Engineering. DOI: 10.1002/9780470686652.eae532
- Iljaszewicz, P., Łusiak, T., et. al., 2020. Aerodynamic analysis of the aircraft model made with the 3D printing method. In Transportation Research procedia. ISSN: 2352-1465. Vol. 51. pp. 118-133. Online: <https://doi.org/10.1016/j.trpro.2020.11.014>.
- Kulkarni, V., Sahoo, N., Chavan, S. D., 2011. Simulation of honeycomb-screen combinations for turbulence management in a subsonic wind tunnel. Journal of Wind Engineering and Industrial Aerodynamics. Vol 99. Issue 1. pp. 37-45. ISSN: 0167-6105. Online: <https://doi.org/10.1016/j.jweia.2010.10.006>.
- Łusiak, T., Novak, A., et. al., 2020. Assessment of impact of aerodynamic loads on the stability and control of the gyrocopter model. In Communications – Scientific Letters of the University of Zilina, Vol. 22 No. 4. pp. 63-69. Online: <https://doi.org/10.26552/com.C.2020.4.63-69>
- Mauro, S., Brusca, S., Lanzafame, R., et. al., 2017. Small-Scale Open-Circuit Wind Tunnel: Design Criticia, Construction and Calibration. International Journal of Applied Engineering Research. Vol 12. Number 23. pp. 13649-13662. ISSN: 0973-4561
- Metha, R. D., Bradshaw P., 1979. Design Rules for Small low Speed Wind Tunnels. Journal of Royal Aeronautical Society. Vol. 73. DOI: 10.1017/S0001924000031985
- Panda, M. K. & Samanta, A. K., 2016. Design of Low Cost Open Circuit Wind Tunnel – A Case Study. Indian Journal of Science and Technology. Vol 9. ISSN: 0974-6846.
- Pecho, P., Ažaltovič, V., et. al., 2019. Introduction of design and layout of UAVs 3D printed wings in relation to optimal

lightweight and load distribution. In Transport Research Procedia. ISSN: 2352-1465. Vol. 40. pp. 861-868. Online: <https://doi.org/10.1016/j.trpro.2019.07.121>.

Škultéty, F., Badánik, B., et. al., 2018. Design of Controllable Unmanned Rescue Parachute Wing. In Transportation Research Procedia. Vol. 35. pp. 220-229. ISSN: 2352-1465. online: <https://doi.org/10.1016/j.trpro.2018.12.026>.

Yang, N. K. C., 2012. Design of Wind Tunnel (FLUID FLOW ANALYSIS). Faculty of Manufacturing Engineering. University Malaysia Pahang. pp. 1-24. Online: <https://core.ac.uk/download/pdf/159179393.pdf>